# Negative-index dispersion and accidental mode degeneracy in an asymmetric spoof–insulator–spoof waveguide*

Li-li Tian(田莉莉)[1], Jian-long Liu(刘建龙)[1], Ke-ya Zhou(周可雅)[1], Yang Gao(高扬)[2], and Shu-tian Liu(刘树田)[1,†]

[1] *Department of Physics, Harbin Institute of Technology, Harbin* 150001, *China*
[2] *College of Electronic Engineering, Heilongjiang University, Harbin* 150080, *China*

(Received 16 January 2017; revised manuscript received 4 April 2017; published online 17 May 2017)

It has been recently demonstrated that negative-index dispersion and mode degeneracy can be achieved by manipulating a spoof–insulator–spoof (SIS) waveguide. In this paper, we propose a new SIS waveguide, which is composed of two spoof surface plasmon polaritons (SSPPs) waveguides drilled with periodic rhomboidal grooves. Both the symmetric and asymmetric cases are investigated. Our simulation results show that the asymmetric SIS waveguides are more significant. By tailoring the tilt of the rhomboidal grooves, the negative-index dispersion can be achieved and the microwave band gap (MBG) can be effectively modulated. At a critical tilt, there appears an accidental mode degeneracy at the edge of the first Brillouin zone. The excitation and propagation of the two coupled modes sustained by the asymmetric SIS waveguides are also demonstrated.

**Keywords:** spoof surface plasmon polaritons, waveguide, negative index, mode degeneracy

**PACS:** 84.40.Az, 84.40.Dc, 78.67.Pt **DOI:** 10.1088/1674-1056/26/7/078401

## 1. Introduction

Surface plasmon polaritons (SPPs) are surface waves that can propagate along a flat metal–insulator interface with high field-confinement.[1,2] In recent decades, considerable effort has been made to develop applications of SPPs in various fields, including materials science,[3] data storage,[4] nanoscale heating,[5] near-field microscopy,[6] biomedical sensing,[7] and so on. One of the main limits in the applications is that the properties of SPPs heavily rely on their frequencies. This is because the metal approximates a perfect electrical conductor (PEC) at low frequencies, for example, terahertz and microwave frequencies. In this case, the flat metal–insulator interface is hard to bound SPPs. Fortunately, an interface with some corrugations can support another surface wave, which is called spoof SPPs (SSPPs) since they have similar dispersion and electromagnetic distributions to SPPs.[8–10] A typical feature of the SSPPs is that they are mainly controlled by the structure parameters instead of materials' permittivity.[11–14] The proposition of SSPPs not only provides a possibility to extend the applications of SPPs to low frequencies, but also adds more degrees of freedom to tailor the plasmonic devices.

A metal surface drilled with periodic rectangular grooves is a typical SSPPs waveguide.[9–11] When two such SSPPs waveguides get close to each other, the SSPPs supported by them will interact, which results in coupled SSPPs. If the two SSPPs waveguides are placed face-to-face, the new waveguide is called a spoof–insulator–spoof (SIS) waveguide.[15–17] It becomes a spoof–metal–spoof (SMS) waveguide if the two SSPPs waveguides face opposite directions.[18–20] Both of the SIS and SMS waveguides can support two kinds of coupled SSPPs modes, whose frequency bands do not overlap each other.[15–20] Introducing geometry modulation to them can generate some interesting phenomena, including negative-index dispersion and topological interface states,[19,21,22] which have been demonstrated in metamaterials and photonic crystals.[23–25] In particular, reference [19] demonstrated experimentally the propagation of coupled SSPPs with negative group velocities. In Ref. [26], Quesada *et al.* proposed an asymmetric SIS waveguide. Through this waveguide, they not only obtained the negative-index dispersion but also achieved mode degeneracy, which is attributed to a higher symmetry of the system.[26]

In this paper, we present and explore another asymmetric SIS waveguide. First, we discuss and analyze an SSPPs waveguide, which is composed of an ultrathin metal strip and periodic rhomboidal grooves. Then a symmetric SIS waveguide and an asymmetric SIS waveguide composed of the SSPPs waveguides are introduced and investigated. We find that the negative-index dispersion and mode degeneracy can be realized on the asymmetric waveguide by tailoring the structure parameters. The difference from Ref. [26] is that the mode degeneracy we achieved is accidental. Finally, we demonstrate the excitation and propagation of the coupled modes in the asymmetric SIS waveguide.

*Project supported by the National Basic Research Program of China (Grant No. 2013CBA01702) and the National Natural Science Foundation of China (Grant Nos. 61377016, 61575055, 10974039, 61307072, 61308017, and 61405056).

†Corresponding author. E-mail: stliu@hit.edu.cn

© 2017 Chinese Physical Society and IOP Publishing Ltd 

## 2. Dispersion for the SSPPs waveguide

Figure 1(a) shows a three-dimensional SIS waveguide drilled with rhomboidal grooves. The bottom of the rhomboidal groove is located at the center of a period unit, while the opening shifts aside. The structure parameters are also presented in Fig. 1(a). The parameter $d$ is the periodicity. In this paper, we only consider the microwave region and pick $d = 1$ mm as the unit length. The parameter $t$ is the waveguide thickness in the $z$ direction. As stated in the previous literature, the propagation properties of SSPPs are not sensitive to the waveguide thickness.[27,28] We choose $t = 0.018d$, which is nearly the thickness of a printed circuit board (convenient in experiment operation). The parameters $a$ and $h$ are the horizontal width and vertical height of the rhomboidal groove, respectively. The vertical width of the waveguide, $w$, is always $0.2d$ wider than $h$. The tilt of the rhomboidal groove is expressed by the horizontal shift of its opening relative to its bottom, which is denoted as $s$. Obviously, $s$ ranges from 0 to $(d-a)/2$. In our theoretical calculation, the metal is modeled as a PEC. All the following results are obtained through simulations based on the finite integration method.

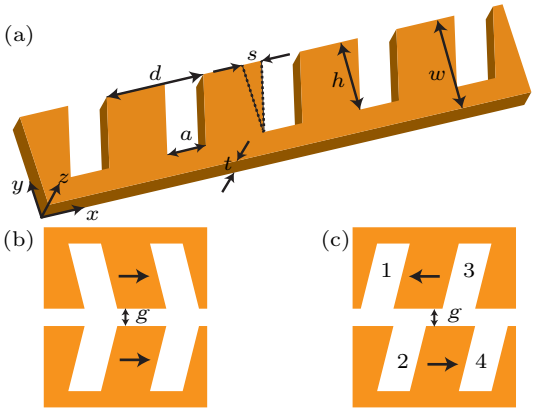



**Fig. 1.** (color online) (a) Schematic of the three-dimensional SSPPs waveguide drilled with periodic rhomboidal grooves. (b) Front view of the symmetric SIS waveguide. (c) Front view of the asymmetric SIS waveguide.

Now we focus on how the tilt influences the properties of the SSPPs supported by the ultrathin waveguide. $h$ and $a$ are set to be $d$ and $0.3d$, respectively. We simulate the dispersion relations at different tilts and show the results in Fig. 2. The black line is the light line, which represents the dispersion relation of light in free space. On its right, the propagation constant $\beta$ is larger than that of free light, resulting in high field-confinement. On the other side, $\beta$ is smaller than that of free light and the waves become radiative. Thus, this region is called a radiation area. It can be seen that all the dispersion curves lie at the right side of the light line, which demonstrates that the SSPPs are confined surrounding the waveguide. As $s$ increases, the dispersion curve moves down, meaning that the field-confinement becomes higher. The reason is that the rhomboidal groove with a bigger tilt is equivalent to a deeper straight rectangular groove.[13] It has been demonstrated that the SSPPs waveguide with deeper straight grooves has a lower frequency band.[10,11]

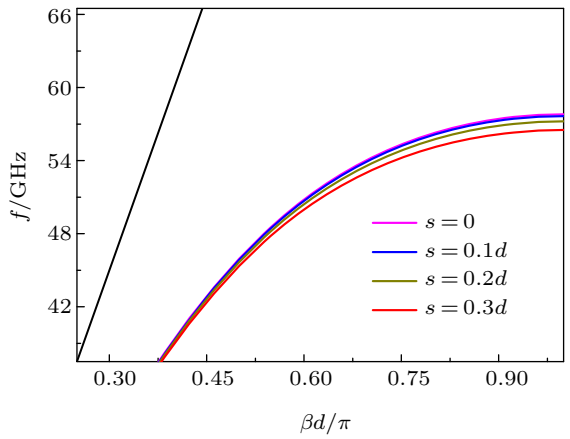



**Fig. 2.** (color online) Dispersion relations of SSPPs on waveguides with rhomboidal grooves, where $d = 1$ mm, $t = 0.018d$, $h = d$, $a = 0.3d$, and $w = h + 0.2d$.

## 3. Dispersion for the SIS waveguide

A pair of the ultrathin SSPPs waveguides discussed above can form an SIS waveguide by placing them face-to-face with a distance of $g$. Two types of SIS waveguides can be obtained by this way. Figure 1(b) shows the front view of the first one. The arrows point the offset direction of the rhomboidal grooves' openings. We can see that the openings of both upper and lower grooves shift to the right. Thus the waveguide features a symmetric geometry. For the second one, the openings of the upper and lower grooves respectively shift to the left and right, as shown in Fig. 1(c). In the SIS waveguides, each individual SSPPs waveguide can support SSPPs. The two layers of SSPPs interact with each other, giving rise to coupled modes. In the following, we explore the coupled modes supported by the two different SIS waveguides.

Firstly, we investigate the symmetric SIS waveguides. The simulated dispersion relations of the coupled modes propagating on them are illustrated in Fig. 3(a) for $s = 0$, $0.1d$, $0.2d$, and $0.3d$. $g$ is fixed at $0.2d$. The curves with the same color correspond to the same $s$. As observed in Fig. 3(a), the dispersion curve of the SSPPs splits into two after coupling. It indicates that the symmetric SIS waveguide can support two coupled modes. Surely, the two coupled modes are in symmetry. The modes with symmetric magnetic field ($z$ component) are called symmetric modes. Their dispersion relations are denoted by the solid curves. The modes with anti-symmetric magnetic field are called anti-symmetric modes, whose dispersion curves are depicted by the dashed curves. The dispersion curves of the symmetric modes are always located on the right of the light line, while those for the anti-symmetric modes pass through the light line and enter the radiation area. The intersections are their cut-off frequencies. There always exists a gap between the two frequency bands, which is the so-called microwave band gap (MBG).[21] The width of the MBG changes little as $s$ increases even though its position has

a little shift. We present the $H_z$ distributions of the two coupled modes on a unit cell of the symmetric SIS waveguide at asymptotic frequencies which correspond to $\beta = \pi/d$ (edge of the first Brillouin zone) in Figs. 3(b) and 3(c) when $s = 0.2d$ and $0.3d$. The left and right panels illustrate the symmetric and anti-symmetric modes, respectively.

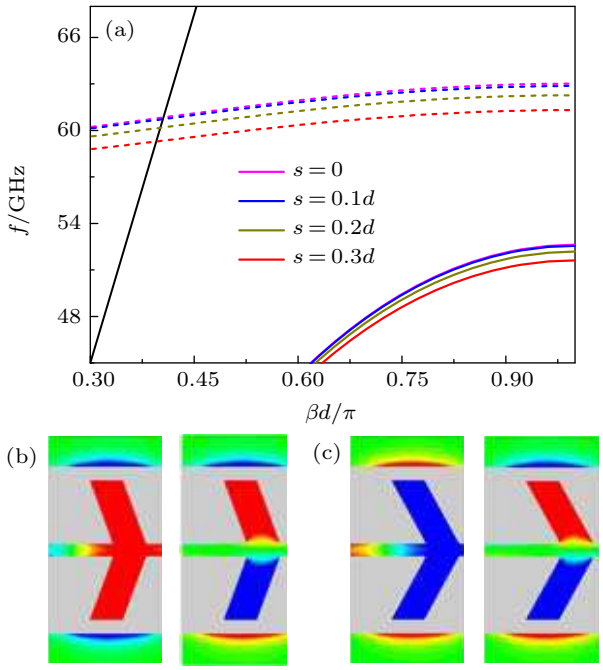



**Fig. 3.** (color online) (a) Dispersion relations of coupled modes on the symmetric SIS waveguides. The solid and dashed curves denote the symmetric and anti-symmetric modes, respectively. (b)–(c) $H_z$ distributions on a unit cell of the symmetric SIS waveguide at asymptotic frequencies when (b) $s = 0.2d$ and (c) $s = 0.3d$. The left and right panels at each subgraph represent the symmetric and anti-symmetric modes, respectively. $d = 1$ mm, $t = 0.018d$, $g = 0.2d$, $a = 0.3d$, $h = d$, and $w = 1.2d$.

Secondly, we analyze the asymmetric SIS waveguides. Figure 4(a) shows the simulated dispersion relations when $s$ changes from 0 to $0.3d$. It can be seen that the asymmetric SIS waveguides also support two coupled SSPPs. We name the two coupled SSPPs symmetric-like and anti-symmetric-like modes in this paper according to their $H_z$ distributions at asymptotic frequencies. The solid and dashed curves in Fig. 4(a) are the dispersion relations of the symmetric-like and anti-symmetric-like modes, respectively. When $s$ is small, the frequency bands of the symmetric-like modes are below those of the anti-symmetric-like modes. As $s$ increases, the dispersion curves of the symmetric-like modes move up, while those of the anti-symmetric-like modes fall down. In this process, the two frequency bands approach each other and the MBG gets effective modulation. Notably, when $s$ exceeds a specific value, the eigen-frequencies of the symmetric-like modes become larger than those of the anti-symmetric-like modes. For the asymmetric SIS waveguide with $s = 0.3d$, the slopes of the dispersion curves of the symmetric-like modes become negative as $\beta$ increases. It indicates that the symmetric-like mode with larger $\beta$ has a negative group velocity. Figures 4(b) and 4(c) present the $H_z$ distributions on a unit cell of the asymmetric SIS waveguide at asymptotic frequencies when $s = 0.2d$ and $0.3d$. The left and right panels correspond to the symmetric-like and anti-symmetric-like modes, respectively.

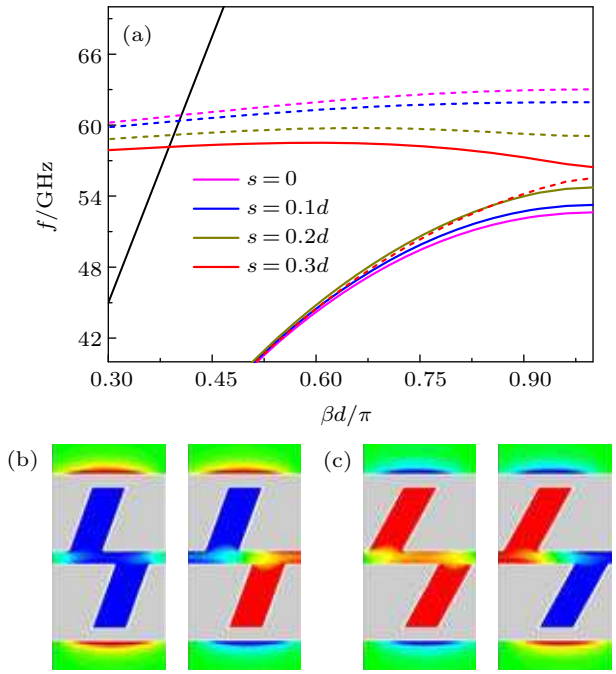



**Fig. 4.** (color online) (a) Dispersion relations of coupled modes on the asymmetric SIS waveguide. The solid and dashed curves denote the symmetric-like and anti-symmetric-like modes, respectively. (b)–(c) $H_z$ distributions on a unit cell of the asymmetric waveguide at asymptotic frequencies when (b) $s = 0.2d$ and (c) $s = 0.3d$. The left and right panels at each subgraph represent the symmetric-like and anti-symmetric-like modes, respectively. $d = 1$ mm, $t = 0.018d$, $g = 0.2d$, $a = 0.3d$, $h = d$, and $w = 1.2d$.

Here, we give a brief analysis. As exhibited in Fig. 1(c), we label four adjacent rhomboidal grooves using 1, 2, 3, and 4, respectively. When $s$ is small, coupling between the SSPPs around the grooves 1 and 2 plays a dominant role. As $s$ increases, the openings of grooves 1 and 2 move away from each other. The dominant coupling strength becomes weak. Thus the dispersion curves of the symmetric-like and anti-symmetric-like modes approach each other. Meanwhile, grooves 2 and 3 get closer. Consequently, the interaction between the SSPPs around them becomes stronger and even exceeds that between grooves 1 and 2 when $s$ is large enough. In this situation, coupling between the SSPPs around grooves 2 and 3 plays a dominant role. If $s$ continues to increase, the dominant coupling strength keeps increasing and the dispersion curves of the two coupled modes begin to leave each other. On the whole, the dispersion curves of the symmetric-like and anti-symmetric-like modes move close to and then away from each other as $s$ increases.

## 4. Mode degeneracy in the asymmetric SIS waveguide

According to our analysis above, there should exist a critical position where the dispersion curves of the two coupled modes are nearest. To find this critical position, we simulate

the evolution of the asymptotic frequencies of the two coupled modes as $s$ increases from 0 to $0.35d$. The results are shown in Fig. 5(a). The solid and dashed curves denote the symmetric-like and anti-symmetric-like modes, respectively. It is noticed that the asymptotic frequency of the symmetric-like mode increases with increasing $s$, while that of the anti-symmetric-like deceases as $s$ increases. The two curves intersect at 56.25 GHz. The corresponding $s$ is $0.283d$, which is the critical position. If $s$ is smaller than $0.283d$, the dispersion curve of the symmetric-like is located below that of the anti-symmetric-like mode. When $s$ is larger than $0.283d$, the positions of the dispersion curves of the two coupled modes are reversed. The region between the blue and red curves corresponds to the MBG of the waveguides. It demonstrates that the MBG can be controlled by the tilt of the rhomboidal grooves effectively.

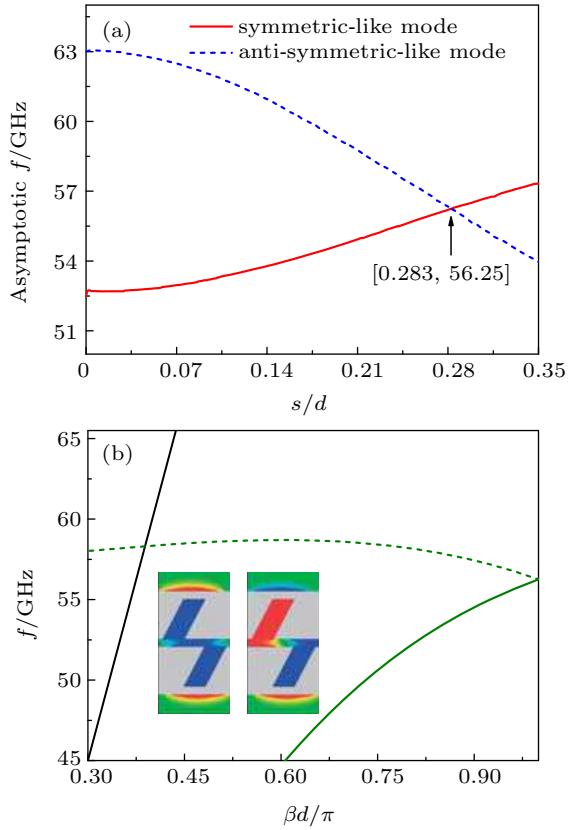



**Fig. 5.** (color online) (a) Asymptotic frequencies of the symmetric-like and anti-symmetric-like modes as a function of $s$. (b) Dispersion relation for the asymmetric SIS waveguide with $s = 0.283d$. Insets in panel (b) are the $H_z$ distributions of the coupled SSPPs on a unit cell of the asymmetric SIS waveguide at 56.25 GHz.

Actually, there appears a mode degeneracy at the intersection. It is easy to find that the asymmetric SIS waveguides we proposed satisfy the screw symmetry $S_z : (x, y, z) \rightarrow (0.5d - x, 0.5 - y, 0.5 + z)$.[29] Unfortunately, the coupled modes on the asymmetric SIS waveguides are confined in the $z$ direction. Thus the screw symmetry here is not responsible for the mode degeneracy of the structures, and the asymmetric SIS waveguides possess no other explicit symmetries. As we have known, the degeneracy appearing in systems that have no symmetries or have hidden symmetries is usually called accidental degeneracy, which means that two or more eigen-states occur at exactly the same frequency only when the geometrical and/or material parameters satisfy certain conditions.[30–32] Therefore, the mode degeneracy in our structures is accidental. It is worth noting that the mode degeneracy in our work is trivial since there is no zero-refractive-index effect at the degeneracy point.

The dispersion relation for the asymmetric SIS waveguide with $s = 0.283d$ is illustrated in Fig. 5(b). As expected, the two dispersion curves touch one point at the edge of the first Brillouin zone. The insets of Fig. 5(b) present the $H_z$ distributions of the coupled modes on a unit cell of the asymmetric SIS waveguide with $s = 0.283d$ at 56.25 GHz. They have different electromagnetic field distributions even though they share the same frequency and propagation constant. It indicates that there appears a mode degeneracy.

Another thing to show that the mode degeneracy is accidental is that the critical $s$ is unpredictable. Now we examine how the groove depth $h$ and space width $g$ influence the critical $s$. First, we fix the space width $g$ at $0.2d$ and simulate changing of the critical $s$ as $h$ varies. Second, we simulate the evolution of the critical $s$ as $g$ changes while $h$ is kept as $d$. The results are shown in Figs. 6(a) and 6(b), respectively. We can see that the critical $s$ decreases as $h$ increases and increases as $g$ increases.

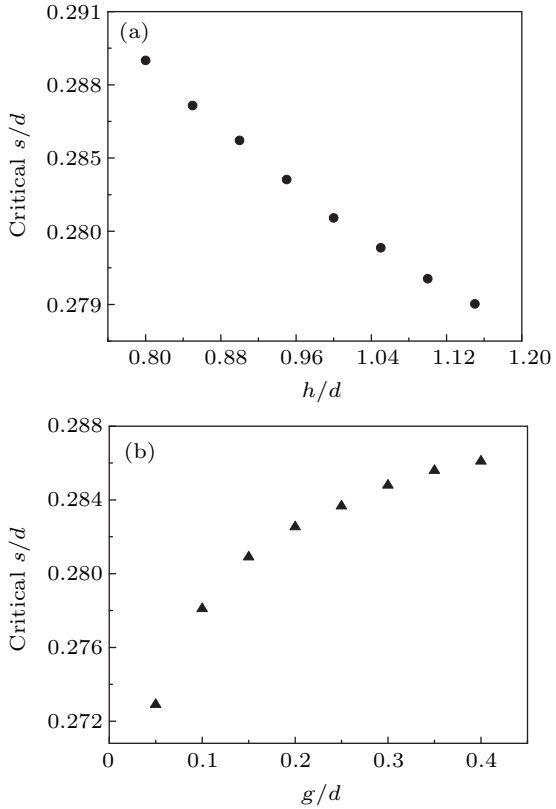



**Fig. 6.** (a) Critical $s$ as a function of the groove depth $h$ when the space width $g$ is fixed at $0.2d$. (b) Critical $s$ as a function of the space width $g$ when the groove depth $h$ is fixed at $d$.

## 5. Excitation and propagation of symmetric-like and anti-symmetric-like modes

In this section, we show the excitation and propagation of coupled modes on an asymmetric SIS waveguide with the help of transitions between a microstrip and a slotline. The proposed structure is illustrated in Fig. 7(a), which consists of a slotline and two microstrips. Figure 7(b) illustrates the front view of the structure. The width and thickness of the slotline are $g$ and $t$, respectively. Its middle part is designed to be an asymmetric SIS waveguide by drilling periodic rhomboidal grooves on it. The depth, width, and tilt of the rhomboidal grooves are $h$, $a$, and $s$, respectively. The two microstrips, depicted by the brown strips, are placed symmetrically at the two sides of the slot line. As shown in Fig. 7(b), they are $0.1d$ below the slotline. There are two ports at the ends of the microstrips serving as the energy sources.

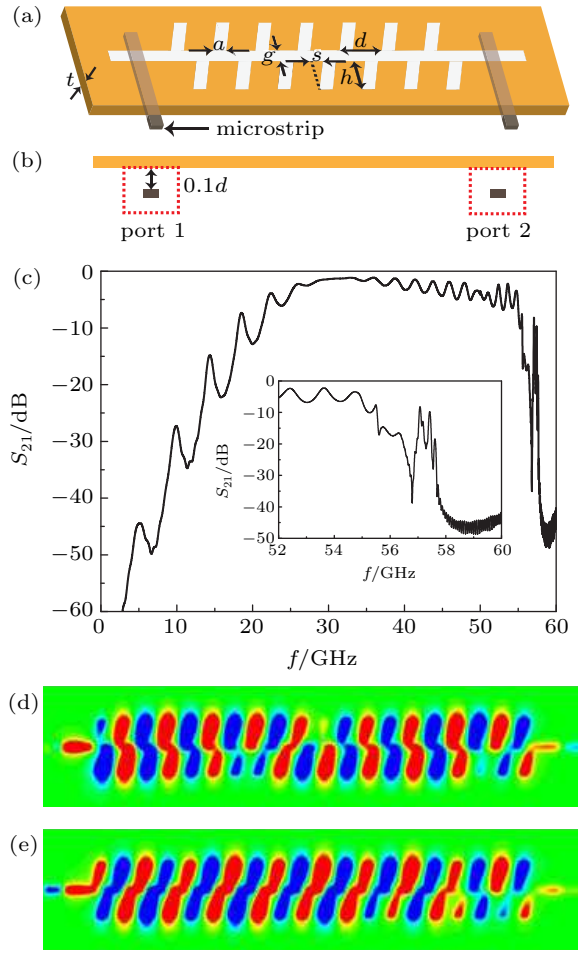



**Fig. 7.** (color online) (a) Three-dimensional diagram of the excitation structure. (b) Front view of the excitation structure. (c) The simulated $S_{21}$ of the excitation structure. (d) $H_z$ distribution of the symmetric-like mode at 56.9 GHz at an $xy$ plane which is $0.1d$ above the structure. (e) $H_z$ distribution of the anti-symmetric-like mode at 55.5 GHz at an $xy$ plane which is $0.1d$ above the structure.

Choosing $g = 0.2d$, $t = 0.018d$, $h = d$, $a = 0.3d$, and $s = 0.3d$, we simulate the $S$ parameters of the excitation system. It should be noted that figure 7(a) just shows a model diagram. The corrugated part of the slotline has 20 periods in our simulation. Figure 7(c) presents the simulated $S_{21}$, which denotes the energy received by port 2 from port 1. Thus $S_{21}$ can express the excitation efficiency of the system. The inset is an enlarged drawing of the results ranging from 50 GHz to 60 GHz. It can be seen that the results are consistent with the dispersion relation shown in Fig. 4(a). Both the symmetric-like and anti-symmetric-like modes can be excited effectively. Figures 7(d) and 7(e) respectively depict the $H_z$ distributions of the symmetric-like and anti-symmetric-like modes at 56.9 GHz and 55.5 GHz at an $xy$ plane which is $0.1d$ above the structure.

## 6. Conclusion

We introduce an ultrathin SSPPs waveguide drilled with periodic rhomboidal grooves. Two such SSPPs waveguides can form a symmetric or an asymmetric SIS waveguide by placing them face-to-face. Both the symmetric and asymmetric SIS waveguides can support two coupled SSPPs modes. There exists an MBG between the frequency bands of the two coupled modes. By tailoring the tilt of the rhomboidal grooves, the MBG of the asymmetric SIS waveguide can be manipulated effectively. Meanwhile, the coupled modes with negative-index dispersion can be achieved. There is a critical tilt. For the asymmetric SIS waveguide with the critical tilt, the MBG disappears and accidental mode degeneracy occurs at the asymptotic frequency. It indicates that the asymmetric SIS waveguides discussed in this paper possess some features of metamaterials and photonic crystals. By using the transitions of a slotline and two microstrips, the excitation and propagation of the two coupled modes supported by the asymmetric SIS waveguides are realized successfully and effectively. We believe that our proposal and investigation are promising for further development of plasmonic devices.

## References

[1] Barnes W L, Dereux A and Ebbesen T W 2003 *Nature* **424** 824
[2] Maier S A 2007 *Plasmonics: Fundatmentals and Applications* (1st Edn.) (New York: Springer) pp. 5–34
[3] Schurig D, Mock J J, Justice B J, Cummer S A, Pendry J B, Starr A F and Smith D R 2006 *Science* **314** 977
[4] Hu H F, Ji D X, Zeng X, Liu K and Gan Q Q 2013 *Sci. Rep.* **3** 1249
[5] Baffou G and Quidant R 2013 *Laser Photon. Rev.* **7** 171
[6] Hohenau A, Krenn J R, Drezet A, Mollet O, Huant S, Genet C, Stein B and Ebbesen T W 2011 *Opt. Express* **19** 25749
[7] Homola J 2008 *Chem. Rev.* **108** 462
[8] Pendry J B, Martin-Moreno L and Garcia-Vidal F J 2004 *Science* **305** 847
[9] Garcia-Vidal F J, Martin-Moreno L and Pendry J B 2005 *J. Opt. A: Pure Appl. Opt.* **7** S97
[10] Shen L F, Chen X D and Yang T J 2008 *Opt. Express* **16** 3326
[11] Liu X Y, Feng Y J, Zhu B, Zhao J M and Jiang T 2013 *Opt. Express* **21** 31155
[12] Shi H Y, Zhang A X, Chen J Z, Wang J F, Song X and Xu Zhuo 2016 *Chin. Phys. B* **25** 78105

[13] Tian L L, Liu J L, Zhou K Y, Gao Y and Liu S T 2016 *Sci. Rep.* **6** 32008
[14] Liu X Y, Zhu L and Feng Y J 2016 *Chin. Phys. B* **25** 34101
[15] Kats M A, Woolf D, Blanchard R, Yu N F and Capasso F 2011 *Opt. Express* **19** 14860
[16] Woolf D, Kats M A and Capasso F 2014 *Opt. Lett.* **39** 517
[17] Tian L L, Chen Y, Liu J L, Guo K, Gao Y and Liu S T 2016 *Chin. Phys. B* **25** 078401
[18] Xu B Z, Li Z, Liu L L, Xu J, Chen C and Gu C Q 2016 *J. Opt. Soc. Am. B* **33** 1388
[19] Liu X Y, Feng Y J, Zhu B, Zhao J M and Jiang T 2016 *Sci. Rep.* **6** 20448
[20] Pang Y Q, Wang J F, Ma Hua, Feng M D, Xia S, X Zhuo and Qu S B 2016 *Appl. Phys. Lett.* **108** 194101
[21] Zhang Q, Xiao J J, Han D Z, Qin F F, Zhang X M and Yao Y 2015 *J. Phys. D: Appl. Phys.* **48** 205103
[22] Meng Y, Xiang H, Zhang R Y, Wu X X, Han D Z, Chan C T and Wen W J 2016 *Opt. Lett.* **41** 3698
[23] Xiao M, Zhang Z Q and Chan C T 2014 *Phys. Rev. X* **4** 021017
[24] Blanco-Redondo A, Andonegui I, Collins M J, Harari G, Lumer Y, Rechtsman M C, Eggleton B J and Segev M 2016 *Phys. Rev. Lett.* **116** 163901
[25] Soukoulis C M and Wegener M 2011 *Nat. Photon.* **5** 523
[26] Quesada R, Martin-Cano D, Garcia-Vidal F J and Bravo-Abad J 2014 *Opt. Lett.* **39** 2990
[27] Shen X P, Cui T J, Martin-Cane D and Garcia-Vidal F J 2013 *Proc. Natl. Acad. Sci. USA* **110** 40
[28] Shen X P and Cui T J 2013 *Appl. Phys. Lett.* **102** 211909
[29] Wang H X, Chen Y G, Hang Z H, Chen H Y, Kee H Y and Jiang J H 2016 arXiv:1608.02437v2.
[30] Huang X Q, Lai Y, Hang Z H, Zheng H H and Chan C T 2011 *Nat. Mater.* **24** 18059
[31] Chen Z G, Ni X, Wu Y, He C, Sun X C, Zheng L Y, Lu M H and Chen Y F 2014 *Sci. Rep.* **4** 4613
[32] Xu L, Wang H X, Xu Y D, Chen H Y and Jiang J H 2016 *Opt. Express* **24** 18059